LARGE-EDDY SIMULATION OF TURBULENCE–RADIATION INTERACTIONS IN A TURBULENT PLANAR CHANNEL FLOW

Ankur Gupta, Michael F. Modest* **and Daniel C. Haworth**

Department of Mechanical and Nuclear Engineering,

The Pennsylvania State University

University Park, PA 16802, USA

ABSTRACT

Large-eddy simulation (LES) has been performed for planar turbulent channel flow between two infinite, parallel, stationary plates. The capabilities and limitations of the LES code in predicting correct turbulent velocity and passive temperature field statistics have been established through comparison to DNS data from the literature for nonreacting cases. Mixing and chemical reaction (infinitely fast) between a fuel stream and an oxidizer stream have been simulated to generate large composition and temperature fluctuations in the flow; here the composition and temperature do not affect the hydrodynamics (one-way coupling). The radiative transfer equation is solved using a spherical harmonics (P1) method, and radiation properties correspond to a fictitious gray gas with a composition- and temperature-dependent Planck-mean absorption coefficient that mimics that of typical hydrocarbon-air combustion products. Simulations have been performed for different optical thicknesses. In the absence of chemical reactions, radiation significantly modifies

*Fellow ASME; Corresponding author; Email: mfmodest@psu.edu

the mean temperature profiles, but temperature fluctuations and turbulence–radiation interactions (TRI) are small, consistent with earlier findings. Chemical reaction enhances the composition and temperature fluctuations, and hence the importance of TRI. Contributions to emission and absorption TRI have been isolated and quantified as a function of optical thickness.

Keywords: Large-eddy Simulation, Thermal Radiation, Turbulence–Radiation Interactions, Chemical Reaction, Channel Flow

1 INTRODUCTION

Most practical combustion systems involve turbulent flow and operate at high temperatures where thermal radiation acts as an important mode of heat transfer. In such systems there are highly nonlinear interactions between chemistry, turbulence, and thermal radiation. Accurate treatment of chemistry, radiation and turbulence in turbulent reacting flow, even without interactions, are quite challenging and complex on their own; therefore, the interactions between turbulence and radiation (turbulence–radiation interactions, TRI) have traditionally been ignored in the modeling of turbulent reacting flows.

TRI arise due to highly nonlinear coupling between the fluctuations of temperature, radiative intensity and the species concentrations. TRI take place over a wide range of length scales. A complete treatment requires consideration of the full range of scales, which is computationally intractable for flows with high Reynolds number, as is the case with chemically reacting turbulent flows of practical interest. Numerical simulation of such systems requires either computing the mean flow while modeling the effects of fluctuations at all scales (Reynolds-averaged approach), or explicitly resolving the large scales while modeling the effects of subfilter-scale fluctuations (Large-Eddy Simulation - LES approach). LES is expected to be more accurate and general, since the large, energy-containing, flow-dependent scales are captured explicitly and only the (presumably) more universal small-scale dynamics require modeling. LES is also expected to capture phe-

nomena that are difficult to accommodate in Reynolds-averaged approaches, such as large-scale unsteadiness. There is a wide and rapidly growing body of evidence that demonstrates quantitative advantages of LES in modeling studies of laboratory flames [1, 2] and in applications to gas-turbine combustors [3–5], IC engines [6–8], and other combustion systems. LES, therefore, promises to be accurate and computationally feasible tool for investigations of TRI in chemically reacting, turbulent flows.

The importance of TRI has long been recognized [9–16]. Studies have shown that the effects of TRI can be as significant as those of turbulence−chemistry interactions. TRI is known to result in higher heat loss due to increased radiative emission, reduced temperatures and, consequently, significant changes in key pollutant species (particularly NOx and soot) in chemically reacting turbulent flows. Faeth and Gore and coworkers [12–16] have shown that, with the inclusion of TRI, radiative emission from a flame may be 50% to 300% higher (depending on the type of fuel) than that expected with radiation but no TRI. With consideration of TRI Coelho [17] reported a nearly 50% increase in radiative heat loss for a nonpremixed methane-air turbulent jet flame; Tessé et al. [18] reported a 30% increase in the radiative heat loss for a sooty nonpremixed ethylene-air turbulent jet flame. Modest and coworkers [19, 20] observed about 30% increase in the radiative heat flux with TRI in their studies of nonpremixed turbulent jet flames. Wu et al. [21] conducted direct numerical simulation (DNS) of an idealized one-dimensional premixed turbulent flame to study TRI along with a high-order photon Monte Carlo scheme (of order commensurate with the underlying DNS code) to calculate the radiative heat source. They isolated and quantified the various contributions to TRI for different optical thicknesses. Deshmukh et al. [22] applied the same approach to DNS of an idealized, statistically homogeneous, nonpremixed system with full consideration of TRI. Frankel et al. [23] performed large-eddy simulation of an idealized nonpremixed jet flame using the optically thin eddy approximation [24] and treating emission TRI through a filtered mass density function (FMDF) approach. Coelho [25] surveyed various computational approaches to account for TRI and reviewed TRI studies based on those approaches.

In this work large-eddy simulation with a P1 radiation model is used to isolate and quantify TRI effects for a range of optical thicknesses for nonreacting and reacting channel flow configurations. The objectives are to provide fundamental physical insight into TRI in chemically reacting flows and to provide guidance for model development, and to establish the suitability of LES for investigating TRI in chemically reacting flows. The remainder of this paper is organized as follows: Section 2 presents the underlying theory behind turbulent–radiation interactions; the problem formulation is outlined in Section 3; results and discussion for the two configurations are presented in Section 4, followed by conclusions in Section 5.

2 THERMAL RADIATION AND TURBULENCE–RADIATION INTERACTIONS (TRI)

The radiative source term in the instantaneous energy equation is expressed as the divergence of the radiative heat flux. For a gray medium,

$$\nabla \cdot \vec{q}_{rad} = 4\kappa_P \sigma T^4 - \kappa_P G \tag{1}$$

where κ_P is the Planck-mean absorption coefficient, σ is the Stefan-Boltzmann constant, and $G \equiv \int_{4\pi} I d\Omega$ is the direction-integrated intensity, or incident radiation, which is obtained by solving the radiative transfer equation (RTE) [26]. The radiative source term consists of an emission part and an absorption part: these are the first and second terms on the right-hand side of Eq. (1), respectively.

TRI can be brought into evidence by taking the mean of Eq. (1):

$$\langle \nabla \cdot \vec{q}_{rad} \rangle = 4\sigma \langle \kappa_P T^4 \rangle - \langle \kappa_P G \rangle \tag{2}$$

In the emission term, TRI appears as a correlation between the Planck-mean absorption coefficient

and the fourth power of temperature: $\langle \kappa_P T^4 \rangle = \langle \kappa_P \rangle \langle T^4 \rangle + \langle \kappa_P' (T^4)' \rangle$, where a prime denotes a fluctuation about the local mean. The presence of TRI in the emission term is further manifested in the temperature self-correlation ($\langle T^4 \rangle \neq \langle T \rangle^4$). In the absorption term, TRI appears as a correlation between the Planck-mean absorption coefficient and the incident radiation: $\langle \kappa_P G \rangle = \langle \kappa_P \rangle \langle G \rangle + \langle \kappa_P' G' \rangle$.

In the present study, we explore the effects of resolved-scale fluctuations on mean and rms temperature profiles and their contribution to TRI using LES. With $\tilde{}$ denoting a filtered (resolved-scale) value, the principal quantities examined are the mean ($\langle \tilde{T} \rangle$) and rms ($\langle \tilde{T}'^2 \rangle$) temperature profiles, the normalized temperature self-correlation ($\langle \tilde{T}^4 \rangle / \langle \tilde{T} \rangle^4$), the Planck-mean absorption coefficient and simplified Planck function (i.e., T^4) correlation ($\langle \widetilde{\kappa_P} \tilde{T}^4 \rangle / \langle \widetilde{\kappa_P} \rangle \langle \tilde{T}^4 \rangle$), and the Planck-mean absorption coefficient and incident radiation correlation ($\langle \widetilde{\kappa_P} \tilde{G} \rangle / \langle \widetilde{\kappa_P} \rangle \langle \tilde{G} \rangle$). In the absence of TRI, each of the latter two quantities would be equal to unity. The expression for temperature self-correlation indicates that in the presence of thermal radiation there would always be TRI for the level of turbulent fluctuations seen in reacting flows. The departures of each of the correlations, stated above, from unity allow different contributions to TRI to be isolated and quantified. In the remainder of the paper, the $\tilde{}$ notation is dropped for clarity, and all quantities correspond to resolved-scale values, unless noted otherwise.

A nondimensional optical thickness $\kappa_P L$ is introduced, where L is an appropriate length scale. Previous studies [24, 27, 28] have suggested that the fluctuations in κ_P (determined by local properties) and in incident radiation G (a nonlocal quantity) are uncorrelated (i.e., $\langle \kappa_P G \rangle \approx \langle \kappa_P \rangle \langle G \rangle$) if the mean free path for radiation is much larger than the turbulence eddy scale. This is the optically thin fluctuation approximation, or OTFA ($\kappa_P L \ll 1$). At the other extreme ($\kappa_P L \gg 1$), the optical thickness may be large compared to all hydrodynamic scales and chemical scales. In that case, the fluctuations in intensity are generated locally and are expected to be correlated strongly with those of the absorption coefficient. A diffusion approximation [26] can be used to model such cases. Between the two extremes are the cases where the smallest scales (Kolmogorov scales and/or flame

thickness) are optically thin while the largest (integral scales) are optically thick. Modeling of such transitional cases is an outstanding challenge in TRI, and is a primary motivation for this study.

3 PROBLEM FORMULATION

Geometric Configuration

A statistically stationary and one-dimensional turbulent planar channel flow is considered. Turbulent channel flow is a classic configuration in the study of fluid dynamics, and has been the subject of numerous DNS and LES investigations [29–32]. This configuration has also been used to study passive scalar statistics [33]. Moreover, a channel domain is a logical extension of classical one-dimensional 'slab' problems often used in the study of radiation heat transfer.

The computational domain is a rectangular box with dimensions (2π, 2, π) in some unit H in the $x-$, $y-$ and $z-$directions, respectively (Fig. 1), with solid boundaries at the bottom ($y = -H$) and top ($y = +H$). Mean-flow statistics vary only in the wall-normal direction (y). Periodic boundaries are used in the streamwise (x) and the spanwise (z) directions for flow. The flow is driven by an artificial streamwise body force that balances the friction at the walls, thus allowing the pressure to be periodic with zero mean pressure gradient in the computational domain. Two cases are considered: a nonreacting case, and a reacting case.

Physical and Numerical Models

CFD Code OpenFOAM [34, 35], an open-source CFD code, has been used to perform the large-eddy simulation for this configuration. The code has been validated by comparing computed mean and rms velocity profiles with published DNS data from the literature for the same Reynolds number ($Re_\tau = 180$, where Re_τ is a Reynolds number based on the wall-friction velocity) [29]. This included a mesh-size and time step sensitivity study, and a comparison of results obtained in the presence or absence of an explicit subfilter-scale (SFS) turbulence model [36]. A second study confirmed that computed mean and rms passive scalar statistics are in good agreement with DNS

data [33]. While the code might not suffice for high-fidelity LES of near-wall turbulence dynamics, it is quite satisfactory for generating a reasonable level of temperature and composition fluctuations for the present purpose of studying thermal radiation and TRI. Quantitative comparisons between LES and DNS mean and rms temperature (passive scalar) profiles are shown in Fig. 2. There is excellent agreement between the LES mean temperature profiles and the DNS data. The mean temperature profile has a steep gradient near the walls due to the formation of turbulent boundary layers and is relatively flat in the core of the channel as a result of turbulent mixing. The rms profiles of temperature fluctuations are normalized by the wall friction temperature (T_τ), which is defined as [33]

$$T_\tau = \frac{q_w}{\rho c_P u_\tau} = \frac{k}{\rho c_P u_\tau} \frac{d\langle T \rangle}{dy}\bigg|_{wall} . \tag{3}$$

Here q_w is the wall heat flux, c_P is the specific heat, k is the thermal conductivity, and u_τ is the wall-friction velocity. The LES rms temperature profile in the absence of a subfilter-scale (SFS) model is within 10% of the DNS data. The maximum temperature fluctuations are at the centerline of the channel, in contrast to the near-wall maximum that is seen for the velocity fluctuations [29]. This is due to the nonzero mean temperature gradient at the centerline of the channel, which results in the production of temperature fluctuations at that location.

Based on the above validation studies, all simulations reported here were performed with no explicit subfilter-scale model using second-order spatial (central differencing) and temporal (Crank-Nicholson) discretizations. This corresponds to the Monotone Integrated LES (MILES) approach for SFS modeling [37], where the SFS model is implicit in the numerical method. The finite-volume grid used has 30, 60 and 50 cells in the $x-$, $y-$ and $z-$directions, respectively, for the nonreacting case and 60, 96 and 60 cells in the $x-$, $y-$ and $z-$directions, respectively, for the re-

acting case. The computational time step corresponds to a maximum material Courant number of 0.3.

Physical Models An incompressible formulation is used. There is no feedback of thermochemistry to the hydrodynamics. The body force and fluid properties are set to achieve the desired Reynolds number ($Re_\tau = 186$) [33], where Re_τ is defined as

$$Re_\tau = \frac{u_\tau H}{\nu} \ , \tag{4}$$

u_τ is given by $\sqrt{\tau_w/\rho}$, and τ_w is the shear stress at the wall. The kinematic viscosity, ν, is calculated using Eq. (4) with u_τ equal to unity. The wall-friction velocity, u_τ, is also used to determine the total wall friction and thus the magnitude of the streamwise body force that is required to sustain the flow.

For the nonreacting case, the top and bottom walls are isothermal at temperatures of 900 K and 1500 K, respectively (Fig. 1a). The laminar Prandtl number is set to 0.7. The channel boundaries in the spanwise and streamwise directions are periodic. The top and bottom walls are treated as black and diffuse for thermal radiation computations. The participating medium has a Planck-mean absorption coefficient of the form

$$\kappa_p = C_\kappa\left[c_0 + c_1\left(\frac{A}{T}\right) + c_2\left(\frac{A}{T}\right)^2 + c_3\left(\frac{A}{T}\right)^3 + c_4\left(\frac{A}{T}\right)^4 + c_5\left(\frac{A}{T}\right)^5\right] \tag{5}$$

where the coefficients c_0 to c_5 and A have been taken from a radiation model suggested for water vapor [38]. Here C_κ is a coefficient that allows the optical thickness to be varied systematically

and independently of the other parameters. The values of C_κ used in this study are: 0.0005, 0.005, 0.05, 2.5, and 50. The Planck-mean absorption coefficient has an inverse temperature dependence and it varies up to a factor of three over the temperature range of interest.

For the reacting case, the species fields are superposed on the flow field; i.e., the hydrodynamics is solved as in the nonreacting case and the flow field is used to transport species through the channel. The species and the energy variables are periodic only for the channel boundaries in the spanwise direction; fixed-value inlet and zero-gradient outlet boundaries are used in the streamwise directions for species and energy variables.

A nonpremixed system with one-step, irreversible, infinitely fast chemistry is considered:

$$F + O \rightarrow P \tag{6}$$

A conserved scalar mixture fraction formulation is used where $\xi = 0.0$ for pure oxidizer, $\xi = 1.0$ for pure fuel, and $\xi = \xi_{st} = 0.5$ for pure products. The Lewis number is set to unity.

A mixture-fraction profile is specified at the channel inlet, with $\xi = 1$ (pure fuel) near the upper ($y = +H$) wall, $\xi = 0$ (pure oxidizer) near the lower ($y = -H$) wall, and a narrow transition zone around $y = 0$:

$$\xi = \frac{1}{2}\left(1 + \tanh 15\frac{y}{H}\right) \tag{7}$$

A zero-normal-gradient boundary condition is used for the mixture fraction at the channel outlet, and at the top and the bottom walls. Species mass fractions Y_F, Y_O, and Y_P are simple piecewise linear functions of ξ, as shown in Fig. 3. In the absence of thermal radiation, the temperature also

is a piecewise linear function of mixture fraction, and has a functional dependence exactly similar to that for pure products. This piecewise linear function along with the inlet mixture-fraction profile (Eq. 7) is used to calculate the temperature distribution at the inlet. In the presence of thermal radiation, however, a separate energy (enthalpy) equation is solved. The specific absolute mixture enthalpy h is:

$$h = \sum_{\alpha} \left(h_{\alpha}^{\circ} Y_{\alpha} + C_{p\alpha} Y_{\alpha} [T - 300] \right) \tag{8}$$

where h_{α}° is the formation enthalpy of species α, Y_{α} is its mass fraction, $C_{p\alpha}$ is its specific heat, and T is the temperature. At the channel inlet, a profile for enthalpy is calculated from the above expression and is assigned as the inlet boundary condition. The specific absolute enthalpy is assumed to have a zero gradient at the outlet. The channel walls are thermally insulated; there is zero net heat flux to the wall:

$$q_{rad} + q_{diff} = q_{rad} - k \nabla T \cdot \hat{n} = 0 \tag{9}$$

where q_{rad} is the net radiative heat flux to the wall, q_{diff} is the diffusive heat flux to the wall, and $\hat{n}$ is the outward unit-normal vector at the wall.

The RTE is solved for incident radiation G using a P1 spherical harmonics method, requiring the solution of an elliptic PDE [26],

$$\nabla \cdot (\Gamma \nabla G) = -\kappa_P \, (4\pi I_b - G) \tag{10}$$

Here I_b is the Planck function, and Γ is the optical diffusivity of the medium which for a nonscattering medium, is given by

$$\Gamma = \frac{1}{3\kappa_P} \tag{11}$$

For the reacting case the channel walls again are black and diffuse. The inlet is assumed to act as a black wall at the local temperature. The channel outlet is assumed to be radiatively insulated, with zero gradient for the incident radiation at the outlet boundary.

The participating medium has a Planck-mean absorption coefficient that is similar to Eq. (5), but includes an explicit dependence on product mass fraction (Y_P):

$$\kappa_p = \max\left\{ \mathrm{C}_\kappa \mathrm{Y}_\mathrm{P}\left[\mathrm{c}_0 + \mathrm{c}_1\left(\frac{\mathrm{A}}{\mathrm{T}}\right) + \mathrm{c}_2\left(\frac{\mathrm{A}}{\mathrm{T}}\right)^2 + \mathrm{c}_3\left(\frac{\mathrm{A}}{\mathrm{T}}\right)^3 + \mathrm{c}_4\left(\frac{\mathrm{A}}{\mathrm{T}}\right)^4 + \mathrm{c}_5\left(\frac{\mathrm{A}}{\mathrm{T}}\right)^5\right], \kappa_{\mathrm{Pmin}} \right\} \tag{12}$$

where $\kappa_{P\mathrm{min}}$ is a very small absorption coefficient (~ 0.01). The values of C_κ used in this study are: 0.0008, 0.008, 0.08, 0.16, 0.8, 4, and 16.

4 RESULTS AND DISCUSSION

For each configuration, results are presented for different optical thicknesses τ. Here τ is defined as

$$\tau = \begin{cases} \langle \kappa_P \rangle_{y=0} H, & \text{for the nonreacting case} \\ \\ \displaystyle\int_{-H}^{+H} \langle \kappa_P \rangle \, dy \Big|_{x=2\pi H}, & \text{for the reacting case} \end{cases} \tag{13}$$

where H is the half-channel height and $y = 0$ is the channel center-line location.

In each case, the initial flow field consisted of uniform streamwise velocity with high velocities in the wall-normal and spanwise directions in a small region at the core of the channel to promote the production of turbulence. A statistically stationary turbulent flow field was established by allowing the initial flow field to develop for approximately 100 flow-through times. The temperature (or mixture-fraction in the reacting configuration) field was introduced only after establishing the statistically stationary turbulent flow field. The initial temperature field used in nonreacting configuration was simply a linear profile between the two walls. The initial mixture-fraction field used in reacting configuration was the inlet mixture-fraction profile of Eq. (7) propagated through the entire channel. The temperature field (or mixture-fraction) was then allowed to evolve for approximately 40-50 flow-through times before switching on thermal radiation, and the system was allowed to evolve for another 70-80 flow-through times to establish statistically stationary fields. Averaging was performed over approximately 100 flow-through times to get proper time-averaged statistics.

Configuration I: Nonreacting turbulent planar channel flow

For this statistically stationary and statistically one-dimensional configuration, mean quantities correspond to averages over time and over planes parallel to the walls. Computed mean temperature profiles in the absence of radiation and for different optical thicknesses are shown in Fig. 4. As thermal radiation is introduced, initially (optically very thin medium, $\tau = 0.01$) most of the thermal radiative energy emitted by the hot wall penetrates through the medium and only a small amount is absorbed. The mean temperature increases slightly from the no-radiation case, with the departure increasing steadily from the hot wall to the cold wall. This can be explained from the inverse-temperature-dependence of the Planck-mean absorption coefficient: the low-temperature zones have a higher absorption coefficient. With an increase in optical thickness ($\tau = 0.1$), most of the thermal energy radiated by the hot wall still penetrates through the medium near the hot wall, but is absorbed near the cold wall. In this case, the mean temperature profile deviates significantly from the no-radiation case. As the optical thickness is increased further ($\tau = 1.0$), the medium near the hot wall also has a large absorption coefficient and absorbs some of the radiative energy emitted by the hot wall. For this case, significant radiative energy still reaches the region near the cold wall resulting in large temperature departures from the no-radiation case. A further increase in optical thickness ($\tau = 50$) results in most of the emitted thermal energy getting absorbed in the region near the hot wall, and the departure from the no-radiation mean temperature distribution has a decreasing trend as one moves from hot wall to cold wall. With further increase in the optical thickness ($\tau = 1250$), the medium becomes essentially opaque and any radiation emitted is absorbed locally close to the point of emission, and the mean temperature distribution approaches the no-radiation temperature distribution. In the limit of large optical thickness, thermal radiation acts as a diffusive process with a diffusivity proportional to $4\sigma T^3/3\kappa_R$, where κ_R is a Rosseland-mean absorption coefficient [26]. For large κ_R the diffusivity due to thermal radiation is negligible, and the mean and rms temperature profiles in the optically thick limit are the same as those in the no-radiation case.

Both emission TRI and absorption TRI are negligible for this case (not shown). This is con-

sistent with findings from earlier studies for nonreacting turbulent flows [11, 39, 40] and can be attributed to the relatively low level of temperature fluctuations (approximately 3% of the mean temperatures) that are found in nonreacting flows.

Here the effect of varying optical thickness on a nonreacting high-temperature system has been studied, for optical thicknesses ranging from very thin ($\tau = 0.01$) to very thick ($\tau = 1250$). For comparison, we note that a 7 mm thick high-temperature region ($T \sim 1500\ K$) of typical combustion products (CO_2 and H_2O, at partial pressures of about 0.1 bar) would have an optical thickness of approximately 0.01. On the other hand, a high-temperature region ($T \sim 1500\ K$) about 50 m thick with 10 ppm soot would correspond to an optical thickness of approximately 1000. Thus an optical thickness of 1250 is extremely large, and serves here only to confirm that the model system exhibits the correct behavior in the optically thick limit. In a practical system, an optical thickness of approximately 15 or greater would correspond to an optically thick medium.

Configuration II: Chemically reacting nonpremixed turbulent channel flow

For this configuration, mean quantities vary with both x and y and, thus, mean quantities are estimated by averaging over time and over z. A further averaging is performed about the $y = 0$ plane to take advantage of the statistical symmetry of the problem and to reduce the statistical errors in estimating mean quantities.

The mean temperature profiles at the exit of the computational domain ($x = 2\pi H$) are shown in Fig. 5. The mean temperature peaks at the center of the channel, and drops to 300 K away from the flame. When thermal radiation is considered the flame loses heat due to radiative energy emission that heats up the adiabatic walls. Because of the heat loss from the flame, the flame core temperature is decreased while the temperature of the gas adjacent to the heated walls increases due to the formation of a thermal boundary layer. As the optical thickness increases, the flame loses more heat resulting in higher wall temperatures and further reduction of the flame core mean temperature. However, for very large optical thicknesses, emitted radiation is absorbed locally and

the mean temperature profile returns to that of the no-radiation case.

The rms temperature profiles at $x = 2\pi H$ are shown in Fig. 6 for different optical thicknesses. Turbulent flapping of the flame about the center-plane of the channel causes large variations in temperature near the edges of the flame and gives rise to a double-peak profile. Thermal radiation significantly alters the temperature fluctuations in the core of the flame.

The temperature self-correlation at the exit is shown in Fig. 7. The shape of the profile can be attributed to the two-peak structure of the rms temperature. The location of the peak depends on the level of temperature fluctuations relative to the mean temperature. Like the rms temperatures, initially the temperature self-correlation decreases with increasing optical thickness and, once the optical thickness attains a sufficiently high value, the temperature self-correlation increases again with increasing optical thickness. The temperature self-correlation is found to be significant for all optical thicknesses considered, due to the high level of temperature fluctuations in the presence of chemical reactions.

Figure 8(a) presents the contribution to emission TRI of the correlation between Planck-mean absorption coefficient and fourth power of temperature at the $x = 2\pi H$ location. This contribution to emission TRI is found to be significant for all optical thicknesses studied except for the optically very thin case ($\tau = 0.02$). The behavior and shape of the correlation can be explained from the assumed functional dependence of the Planck-mean absorption coefficient on temperature and Y_P: κ_P is inversely proportional to temperature, but directly proportional to Y_P. Therefore, the fluctuations in temperature and κ_P are negatively correlated at constant Y_P, and fluctuations in product mass fraction and κ_P are positively correlated at constant temperature. These two opposing phenomena compete with one another to determine the overall correlation. In the region near the flame edge the temperature fluctuations have a dominant impact on κ_P fluctuations, thereby resulting in a correlation less than unity. Similarly, in regions slightly away from the flame edge, Y_P fluctuations are dominant resulting in correlations much greater than unity. However, it is important to realize that the region where the κ_P–T^4 correlation is most significant has about two orders

of magnitude lower mean emission than the maximum mean emission, which occurs at $y = 0$, as seen in Fig. 8(b). The κ_P–T^4 correlation is close to unity at $y = 0$, whereas at the same location the temperature self-correlation is close to 2 as seen in Fig. 7. These numbers and the plots for temperature self-correlation, the κ_P–T^4 correlation and for mean heat emission indicate that here the temperature self-correlation is the dominant contributor to emission TRI.

Absorption TRI at $x = 2\pi H$ is shown in Fig. 9(a) for different optical thicknesses, and is seen to be negligible for optically thin flames, consistent with the OTFA (optically thin fluctuation approximation). Absorption TRI becomes significant at higher optical thicknesses; there thermal radiation travels relatively short distances, and the local incident radiation has some correlation with local emission and, therefore, with the local Planck-mean absorption coefficient. Regions where the κ_P–G correlation is most significant have one-to-two orders of magnitude lower mean absorption rates than the maximum mean absorption rate, as seen in Fig. 9(b).

The plots for temperature self-correlation, the κ_P–T^4 correlation and the κ_P–G correlation [Figs. 7, 8(a) and 9(a), respectively] reveal that, in the optically thin limit where $\tau = 0.02$, the temperature self-correlation is primarily the sole contributor to TRI, and it remains an important contributor to TRI for the entire range of optical thickness considered. This is because the temperature self-correlation is significant in the region with large mean emission rates (i.e., $|y| \leq 0.3$) as opposed to the κ_P–T^4 correlation and the κ_P–G correlation which are dominant in the regions with mean rates one or two orders of magnitude lower than the maximum mean emission and mean absorption rates, respectively (see Figs. 8(b) and 8(b)). The κ_P–T^4 correlation is important at all optical thicknesses except in the optically thin limit, whereas absorption TRI (κ_P–G correlation) is important only in the optically intermediate to thick regions. Note that for very large optical thicknesses both emission TRI and absorption TRI are strong, but their net effect is small due to cancellation (Figs. 8 and 9): in the optically thick limit local values of G approach $4\pi I_b$ and, therefore, the fluctuations in G are directly proportional to the fluctuations in T^4. Absorption TRI [Fig. 9(a)] has similar shape and behavior as emission TRI [Fig. 8(a)] for very large optical thick-

nesses. Similarly, it can be seen from the mean emission and mean absorption plots [Figs. 8(b) and 9(b)] that the mean emission rate is identical to the mean absorption rate for very large optical thicknesses, resulting in mean temperatures approaching those of the no-radiation case as seen in Fig. 5.

5 CONCLUSIONS

Large-eddy simulation of incompressible turbulent planar channel flow has been conducted, including thermal radiation. Cases without and with chemical reaction were considered with systematic variation in optical thickness. In the absence of chemical reactions radiation significantly modifies the mean temperature fields, but TRI were found to be negligible. The no-radiation results are recovered in both the optically thin and optically thick limits. With chemical reactions emission TRI is important at all optical thicknesses, while absorption TRI increases with increasing optical thickness. For the present configuration the temperature self-correlation makes the most important contribution to emission TRI. The other noted contribution to emission TRI is Planck-mean absorption coefficient–Planck function correlation. Absorption TRI is as significant as emission TRI at large optical thicknesses, and the two tend to cancel each other out.

Because of the number of simplifications made in this analysis, results from this idealized case should be considered as qualitative. The proposed next steps are: 1) finite-rate chemistry with a filtered density function (FDF) method to accommodate turbulent–chemistry interactions (TCI); 2) nongray thermal radiation properties; and 3) a more accurate radiative transfer equation (RTE) solver such as photon Monte Carlo (PMC) method or a higher-order $P-N$ method.

ACKNOWLEDGMENT

This work has been supported by the National Science Foundation [Grant Number CTS-0121573] and NASA [Award Number NNX07AB40A].

References

[1] H. Pitsch, Improved pollutant predictions in large-eddy simulations of turbulent non-premixed combustion by considering scalar dissipation rate fluctuations, *Proceedings of The Combustion Institute* 29 (2002), 1971–1978.

[2] M. R. H. Sheikhi, T. G. Drozda, P. Givi, F. A. Jaberi and S. B. Pope, Large eddy simulation of a turbulent nonpremixed piloted methane jet flame (Sandia Flame D), *Proceedings of The Combustion Institute* 30 (2005), 549–556.

[3] P. Moin and S. V. Apte, Large-eddy simulation of realistic gas turbine combustors, *AIAA Paper No. AIAA-2004-330* (2004).

[4] S. James, J. Zhu and M. S. Anand, Large-eddy simulations of gas turbine combustors, AIAA Paper no. 2005-0552 (2005).

[5] P. Flohr, CFD modeling for gas turbine combustors, In *Turbulent Combustion* (Edited by L. Vervisch, D. Veynante and J. P. A. J. Van Beeck), von Karman Institute for Fluid Dynamics Lecture Series 2005-02, Rhode-Saint-Genèse, Belgium March 2005.

[6] I. Celik, I. Yavuz and A. Smirnov, Large-eddy simulations of in-cylinder turbulence for IC engines: A review, *Internl. J. Engine Res.* 2 (2001), 119–148.

[7] D. C. Haworth, A review of turbulent combustion modeling for multidimensional in-cylinder CFD, *SAE Transactions, Journal of Engines* (2005), 899–928.

[8] S. Richard, O. Colin, O. Vermorel, A. Benkenida, A. Angelberger and D. Veynante, Towards large-eddy simulation of combustion in spark-ignition engines, *Proceedings of the Combustion Institute* 31 (2007), 3059–3066.

[9] A. A. Townsend, The Effects of Radiative Transfer on Turbulent Flow of a Stratified Fluid, *J. Fluid Mech.* 4 (1958), 361–375.

[10] T.H. Song and R. Viskanta, Interaction of Radiation with Turbulence: Application to a Combustion System, *J. Thermoph. Heat Transfer* 1 (1987), 56–62.

[11] A. Soufiani, P. Mignon and J. Taine, Radiation–Turbulence Interaction in Channel Flows of

Infrared Active Gases, In *Proceedings of the International Heat Transfer Conference*, Vol. 6, pp. 403–408, ASME 1990.

[12] J. P. Gore and G. M. Faeth, Structure and spectral radiation properties of turbulent ethylene/air diffusion flames, In *Twenty-First Symposium (International) on Combustion*, pp. 1521–1531, The Combustion Institute 1986.

[13] J. P. Gore and G. M. Faeth, Structure and Spectral Radiation Properties of Luminous Acetylene/Air Diffusion Flames, *J. Heat Transfer* 110 (1988), 173–181.

[14] M. E. Kounalakis, J. P. Gore and G. M. Faeth, Turbulence/Radiation Interactions in Nonpremixed Hydrogen/Air Flames, In *Twenty-Second Symposium (International) on Combustion*, pp. 1281–1290, The Combustion Institute 1988.

[15] M. E. Kounalakis, Y. R. Sivathanu and G. M. Faeth, Infrared Radiation Statistics of Nonluminous Turbulent Diffusion Flames, *J. Heat Transfer* 113(2) (1991), 437–445.

[16] G. M. Faeth, J. P. Gore, S. G. Shuech and S. M. Jeng, Radiation from Turbulent Diffusion Flames, *Ann. Rev. Numer. Fluid Mech. Heat Trans.* 2 (1989), 1–38.

[17] P. J. Coelho, Detailed Numerical Simulation of Radiative Transfer in a Nonluminous Turbulent Jet Diffusion Flame, *Comb. Flame* 136 (2004), 481–492.

[18] L. Tessé, F. Dupoirieux and J. Taine, Monte Carlo Modeling of Radiative Transfer in a Turbulent Sooty Flame, *Int. J. Heat Mass Transfer* 47 (2004), 555–572.

[19] S. Mazumder and M. F. Modest, A PDF Approach to Modeling Turbulence–Radiation Interactions in Nonluminous Flames, *Int. J. Heat Mass Transfer* 42 (1999), 971–991.

[20] G. Li and M. F. Modest, Application of Composition PDF Methods in the Investigation of Turbulence–Radiation Interactions, *J. Quant. Spectrosc. Radiat. Transfer* 73(2–5) (2002), 461–472.

[21] Y. Wu, D. C. Haworth, M. F. Modest and B. Cuenot, Direct Numerical Simulation of Turbulence/Radiation Interaction in Premixed Combustion Systems, *Proceedings of the Combustion Institute* 30 (2005), 639–646.

[22] K. V. Deshmukh, D. C. Haworth and M. F. Modest, Direct Numerical Simulation of Turbulence/Radiation Interactions in Nonpremixed Combustion Systems, *Proceedings of the Combustion Institute* 31 (2007), 1641–1648.

[23] A. J. Chandy, D. J. Glaze and S. H. Frankel, Mixing Models and Turbulence-Radiation Interactions in Non-Premixed Jet Flames via the LES/FMDF Approach, In *5th US Combustion Meeting, San Diego, CA, March 25-28*, 2007.

[24] V. P. Kabashnikov and G. I. Kmit, Influence of Turbulent Fluctuations on Thermal Radiation, *J. Applied Spectroscopy* 31 (2) (1979), 963–967.

[25] P. Coelho, Numerical Simulation of the Interaction Between Turbulence and Radiation in Reactive Flows, *Progress in Energy and Combustion Science* 33 (2007), 311–383.

[26] M. F. Modest, *Radiative Heat Transfer* (2nd Edn), Academic Press, New York 2003.

[27] V. P. Kabashinikov, Thermal Radiation of Turbulent Flows in the Case of Large Fluctuations of the Absorption Coefficient and the Planck Function, *J. Eng. Phys.* 49(1) (1985), 778–784.

[28] V. P. Kabashinikov and G. I. Myasnikova, Thermal Radiation in Turbulent Flows—Temperature and Concentration Fluctuations, *Heat Transfer-Soviet Research* 17(6) (1985), 116–125.

[29] R. D. Moser, J. Kim and N. N. Mansour, Direct Numerical Simulation of Turbulent Channel Flow up to Re_τ=590, *Physics of Fluids* 11 (4) (1999), 943–945.

[30] K. Horiuti, The Role of the Bardina Model in Large Eddy Simulation of Turbulent Channel Flow, *Physics of Fluids A* 1 (2) (1989), 426–428.

[31] U. Piomelli, P. Moin and J. H. Ferziger, Model Consistency in Large Eddy Simulation of Turbulent Channel Flows, *Physics of Fluids* 31 (1988), 1884–1891.

[32] P. Moin and J. Kim, Numerical Investigation of Turbulent Channel Flow, *J. Fluid Mech.* 118 (1982), 341–377.

[33] B. Debusschere and C. J. Rutland, Turbulent Scalar Transport Mechanisms in Plane Channel and Couette Flows, *Int. J. Heat Mass Transfer* 47 (2004), 1771–1781.

[34] H. G. Weller, G. Tabor, H. Jasak and C. Fureby, A Tensorial Approach to Continuum Mechanics Using Object Oreinted Techniques, *Computers in Physics* 12 (6) (1998), 620–631.

[35] See *www.openfoam.org*, January, 2006.

[36] A. Gupta, Large-Eddy Simulation of Turbulence/Chemistry/Radiation Interactions in Planar Channel Flow, Master's thesis, The Pennsylvania State University, University Park, PA 2007.

[37] J. P. Boris, F. F. Grinstein, E. S. Oran and R. J. Kolbe, New Insights Into Large Eddy Simulation, *Fluid Dynamics Research* 10 (1992), 199–228.

[38] Sandia National Laboratories Combustion Research Facility, *Intern'l. Workshop on Measurement and Computation of Turbulent Nonpremixed Flames* 2002.

[39] S. Mazumder and M. F. Modest, Turbulence–Radiation Interactions in Nonreactive Flow of Combustion Gases, *J. Heat Transfer* 121 (1999), 726–729.

[40] V. Singh, Study of Turbulence Radiation Interactions Using LES of Planar Channel Flow, Master's thesis, The Pennsylvania State University, University Park, PA 2005.

List of Figures

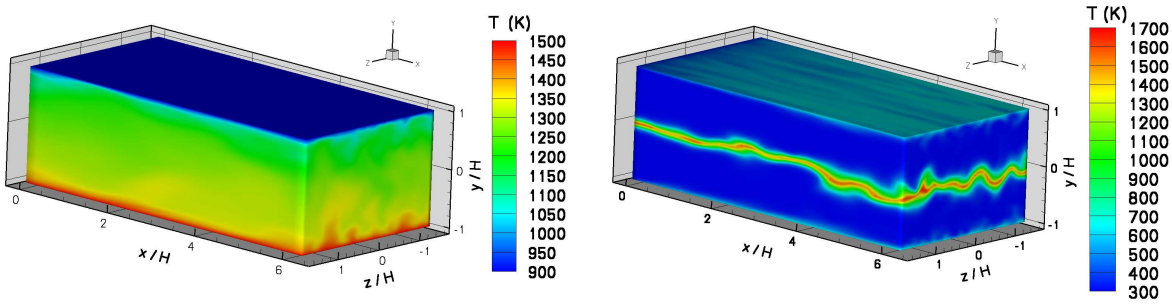

(a) Nonreacting Flow (b) Reacting Flow

Figure 1. Instantaneous temperature contours for (a) nonreacting flow and (b) reacting flow.

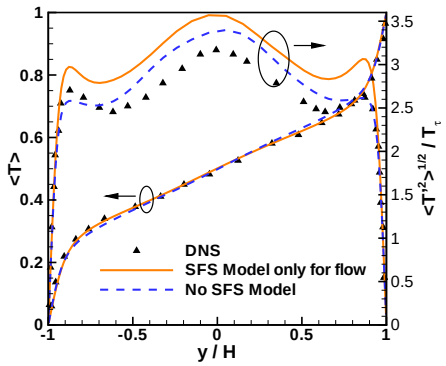

Figure 2. Computed mean and rms passive scalar profiles, and their comparison with DNS of Debusschere and Rutland [33].

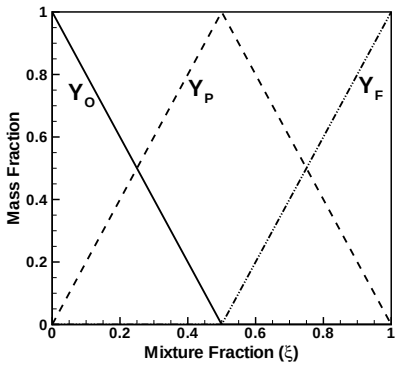

Figure 3. Species mass fractions as a function of mixture fraction, ξ.

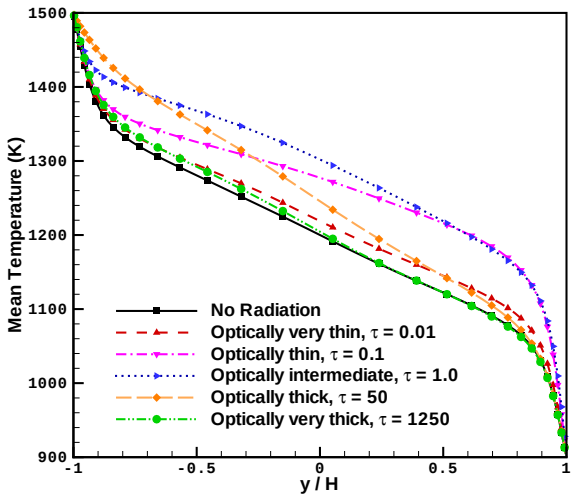

Figure 4. Computed mean temperature profiles with variations in optical thickness for the nonreacting case.

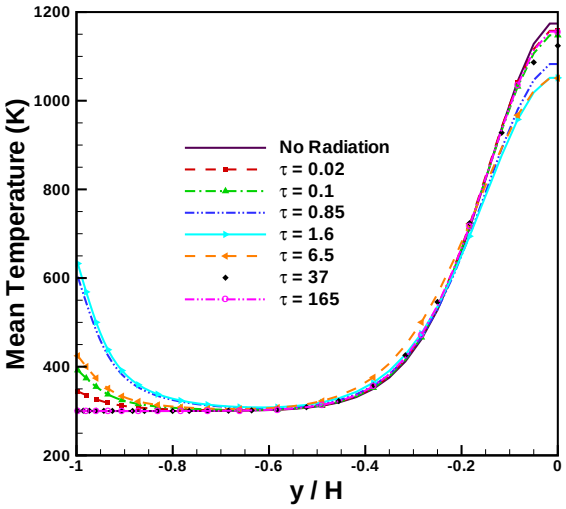

Figure 5. Computed mean temperature profiles with variations in optical thickness for the reacting case.

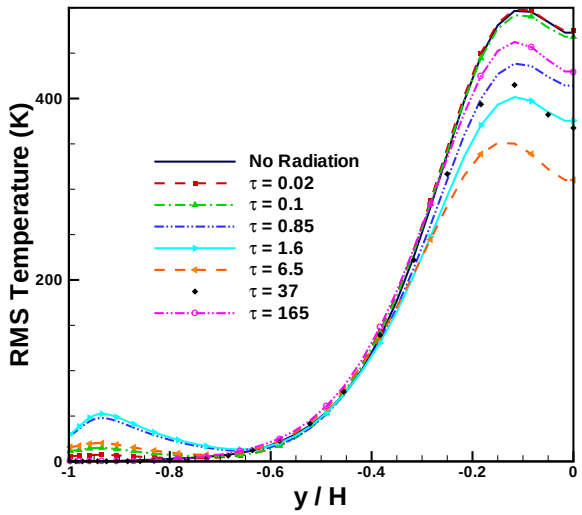

Figure 6. Computed rms temperature profiles with variations in optical thickness for the reacting case.

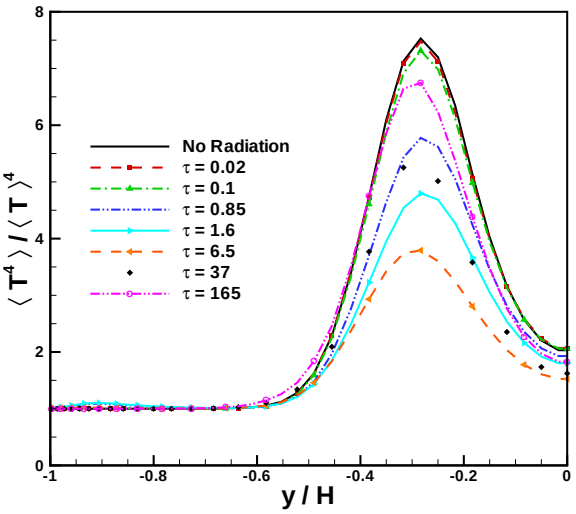

Figure 7. Temperature self-correlation for several optical thicknesses for the reacting case.

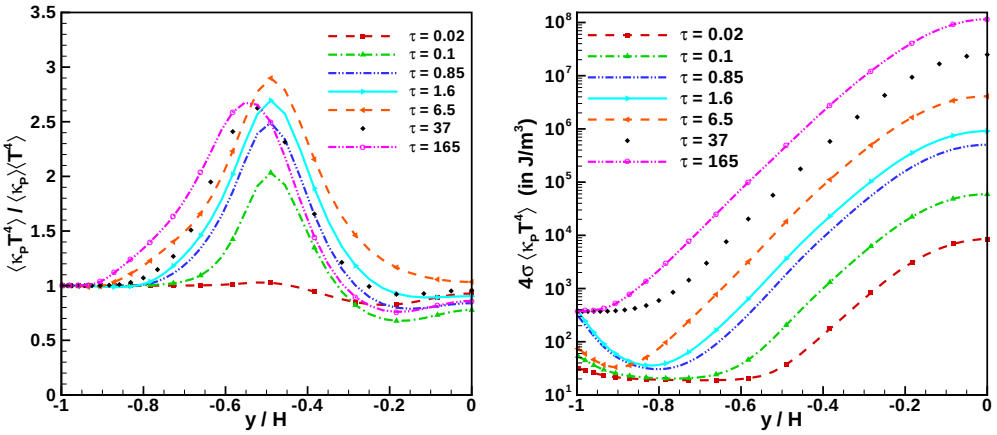

(a) Normalized correlation

(b) Mean radiative heat emission rate per unit volume

Figure 8. Correlation between κ_P and T^4 for several optical thicknesses for the reacting case.

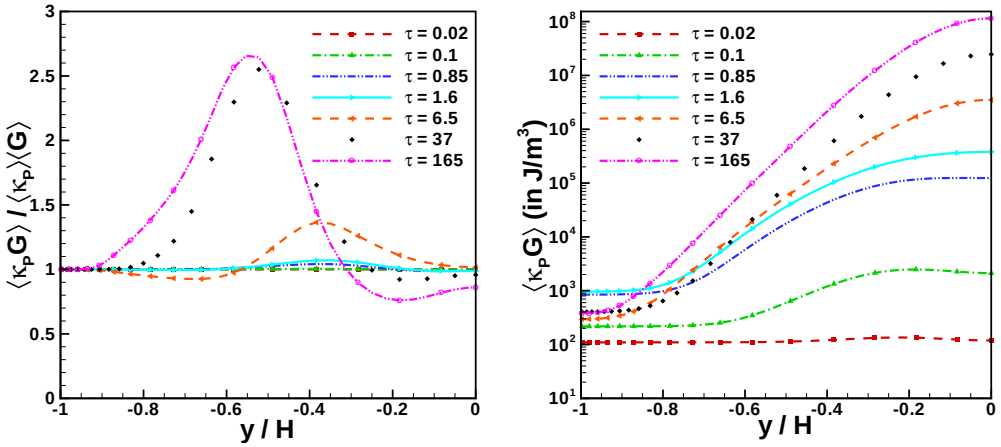

(a) Absorption TRI

(b) Mean radiative heat absorption rate per unit volume

Figure 9. Absorption TRI for several optical thicknesses for the reacting case.